High Density Model Reduction Uncertainty Quantification for Multigroup Diffusion Neutronics

Paul W. Talbot*[1], Anil K. Prinja[1] and Cristian Rabiti[2]

[1]Department of Nuclear Engineering, University of New Mexico
[2]Idaho National Laboratory

December 3, 2014

*talbotp@unm.edu

1 Introduction

There have been many recent advances in uncertainty quantification in numerical models for computational physics [1]. In this document, we present ongoing work to demonstrate the efficiency of high-density model reduction (HDMR) techniques as well as sparse-grid stochastic collocation on sparse grids (SC) [6] in comparison with traditional analog Monte Carlo (MC) uncertainty quantification methods.

2 Motivation

The development of computational numerical models to simulate scientific processes often results in a solver. The solver takes inputs from the user, performs some computational algorithm, and returns some quantity of interest. In our work we label this algorithm the *deterministic solver*, since it should result in a nearly identical value for the quantity of interest as long as the inputs aren't changed. This may be misleading, as the deterministic solver might use a stochastic algorithm like Monte Carlo to solve the system; however, when we speak of deterministic or stochastic solvers, we refer to the input space, not the algorithm itself.

While the deterministic solver is a powerful tool, it often fails to capture aleatory or epistemic uncertainty in the input parameters. Either because of randomness of the physics or uncertainty in measuring the input parameters, an accurate solver should quantify the uncertainty space of the input parameters and the resulting solution space for the quantity of interest. Solely making use of the deterministic solver potentially presents a naive picture of the solution space.

There are two major classes of uncertainty quantification methods, separated by their impact on the deterministic solver itself. Intrusive methods make use of parameter changes within the algorithm, necessitating the deterministic code have uncertainty quantification built-in or added. Non-intrusive methods treat the deterministic solver as a black box to be sampled. This allows the freedom to use the non-intrusive methods on any deterministic solver that requires inputs and delivers a quantity of interest, and will be the focus of our work.

Among non-intrusive methods, we can further divide uncertainty quantification into stochastic and deterministic methods. Stochastic methods are centered around randomly sampling the input parameter uncertainty space and deriving statistics from resulting quantities of interest, and include methods such as analog Monte Carlo, multilevel Monte Carlo, and Latin Hypercube. Deterministic methods sample from the uncertainty space in predefined locations, using characteristic or interpolating polynomials to create a Reduced-Order Model (ROM) of the uncertainty space, and include methods like stochastic Galerkin, stochastic least squares, and stochastic collocation.

Traditionally, Monte Carlo methods are effective at converging but slow to do so. Additionally, Monte Carlo for uncertainty quantification is dimension-agnostic; that is, if we consider N to be the number of uncertain input parameters, Monte Carlo shows the same convergence behavior regardless the size of N. Stochastic collocation is based on using selected quadrature points within the uncertain input space to construct polynomials to represent the quantity of interest solution space, and for a small N and reasonably smooth uncertain input space, converges much more quickly than Monte Carlo. However, the N-dimensional quadrature set grows exponentially with increasing N, forcing collocation to suffer from the curse of dimensionality. In this work, we explore methods to negate

some of the difficulties of increased dimension in collocation methods and show improvement over analog Monte Carlo methods for larger numbers N of uncertain input parameters.

3 Deterministic Model

The uncertainty quantification methods we describe are agnostic of the deterministic problem whose uncertainty is quantified. However, to demonstrate the effectiveness of these methods, we apply uncertainty quantification to three different deterministic solvers: an attenuation problem solver, a projectile with drag range solver, and a nuclear reactor core k-eigenvalue solver.

3.1 Attenuation Problem Solver

Because of its simple but non-parabolic analytic solution, we make use of the attenuation problem to demonstrate convergence to a known benchmark value. This problem simulates the attenuation of a beam of particles through a fixed-size block subdivided into several sections with varying absorption cross sections. The quantity of interest is the exit beam strength, and the problem can be solved analytically as

$$u(Y) = \prod_{n=1}^{N} \exp\left(-\frac{Y_n}{N}\right), \tag{1}$$

where u is the fractional emitted beam strength, N is the number of uncertain cross sections (and also the number of subdivided segments), and $Y = Y_1, \ldots, Y_N \in \Omega$ are the product of uncertain cross sections and unit length, with Ω as the entirety of the combined uncertain input space. If we assign uniform uncertainty to the inputs ranging from a to b, the mean can likewise can be computed analytically as

$$\mathbb{E}[u(Y)] = \int_{\Omega} u(Y)P(Y)d\Omega, \tag{2}$$

$$= \prod_{n}^{N} (b-a)^{-1} \int_{a}^{b} \exp\left(-\frac{Y_n}{N}\right) dY_n, \tag{3}$$

$$= \left[\left(\frac{N}{b-a}\right)\left(e^{-a/N} - e^{-b/N}\right)\right]^N. \tag{4}$$

For this work, $N = 5$, $a = 1$, and $b = 6$.

3.2 Projectile with Drag Problem Solver

This problem is included to demonstrate a problem without direct analytic solution and that uses a grid-based deterministic solver. In this problem we consider the range R of a spherical projectile with mass m, radius r, and drag coefficient C launched from a height of y_i at an angle of θ with respect to parallel with the ground at an initial velocity of v, and density of the air ρ and gravitational acceleration constant g. We allow each of these to vary uncertainly with value as in Table 1.
The equations of motion are given in both the horizontal x and vertical y dimensions as

$$R = \frac{v_t}{g}(v\sin\theta + v_t)\left(1 - e^{-g\ t/v_t}\right) - v_t t, \tag{5}$$

$$x_f = \frac{v\ v_t\cos\theta}{g}\left(1 - e^{-g\ t/v_t}\right), \tag{6}$$

Input	Mean	Range
m	0.145 kg	0.0725 kg
r	0.0336 m	0.00336 m
C	0.5	0.5
ρ	1.2 kg/m^3	0.1 kg/m^3
v	50 m/s	5 m/s
θ	45^o	10^o
g	9.7988 m/s^2	0.0349 m/s^2
y_i	1 m	1 m

Table 1: Projectile with Drag Inputs

$$v_t = \frac{mg}{D}, \qquad D = \frac{\rho C A}{2}, \qquad A = \pi r^2. \tag{7}$$

The deterministic solver for the projectile problem uses a forward-Euler time-stepping scheme, and its accuracy depends strongly on the time step used.

3.3 Reactor Core k-eigenvalue Solver

To demonstrate the uncertainty quantification performance on a difficult, nonlinear problem we introduce a solver for a nuclear reactor core neutronics problem. With this model we solve a two-dimensional nonlinear dual-energy group neutron diffusion criticality benchmark problem [4]. This problem simulates an orthogonal quarter-core reactor by imposing reflective conditions on the left and bottom boundaries, with vacuum no-traction conditions on the top and right. the problem makes use of five materials in 121 regions. Fig. 1 illustrates the core.

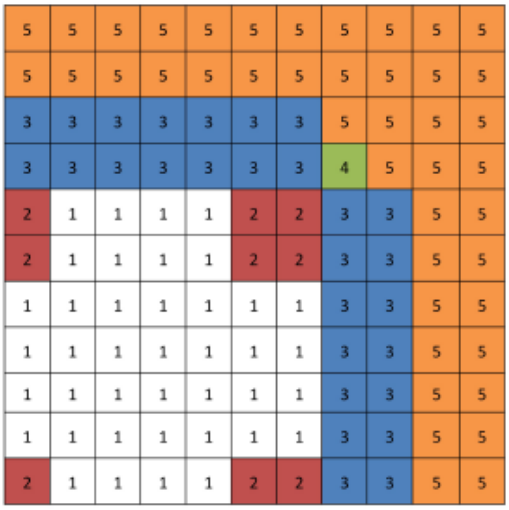

Figure 1: Core Geometry

3.4 Mathematical Model

The PDE describing steady-state neutron transport in the core is the two-group neutron diffusion criticality approximation,

$$-\boldsymbol{\nabla}\cdot(D_1(\bar{x})\boldsymbol{\nabla}\phi_1(\bar{x}))+\Big(\Sigma_a^{(1)}(\bar{x})+\Sigma_s^{(1\to 2)}(\bar{x})\Big)\phi_1(\bar{x})=\frac{1}{k(\phi)}\sum_{g'=1}^{2}\nu_{g'}\Sigma_f^{(g')}(\bar{x})\phi_{g'}(\bar{x}), \tag{8}$$

$$-\boldsymbol{\nabla}\cdot(D_2(\bar{x})\boldsymbol{\nabla}\phi_2(\bar{x}))+\Sigma_a^{(2)}(\bar{x})\phi_2(\bar{x})=\Sigma_s^{(1\to 2)}(\bar{x})\phi_1(\bar{x}), \tag{9}$$

where we use the following parametric coefficients: the absorption cross section $\Sigma_{g,a}=\Sigma_{g,c}+\Sigma_{g,f}$; the capture and fission cross sections $\Sigma_{g,c}$ and $\Sigma_{g,f}$; the diffusion coefficient D_g which depends on the scattering cross section of the medium; and the fission multiplication factor ν_g, the ratio of new neutrons per fission-producing neutron. The solution to this PDE is the neutron scalar flux $\phi_g(\bar{x})$. We apply no-traction conditions on the vacuum boundaries and zero-derivative current on the reflecting boundaries for both energy groups:

$$\frac{\phi_g}{4}-\frac{D_g}{2}\left.\frac{\partial\phi_g}{\partial x_1}\right|_{\partial\Omega_{\text{top}}}=0,\ \ g=1,2, \tag{10}$$

$$\frac{\phi_g}{4}-\frac{D_g}{2}\left.\frac{\partial\phi_g}{\partial x_2}\right|_{\partial\Omega_{\text{right}}}=0,\ \ g=1,2, \tag{11}$$

$$-D_g\left.\frac{\partial\phi_g}{\partial x_1}\right|_{\partial\Omega_{\text{bottom}}}=0,\ \ g=1,2, \tag{12}$$

$$-D_g\left.\frac{\partial\phi_g}{\partial x_2}\right|_{\partial\Omega_{\text{left}}}=0,\ \ g=1,2. \tag{13}$$

The material properties are shown in Table 2, and the domain $\Omega=[0,200\text{ cm}]^2$. The reference flux solutions are plotted in Fig. 2, and for the reference problem k=1.00007605445.

Region	Group	D_g	$\Sigma_{a,g}$	$\nu\Sigma_{f,g}$	$\Sigma_s^{1,2}$
1	1	1.255	8.252e-3	4.602e-3	2.533e-2
	2	2.11e-1	1.003e-1	1.091e-1	
2	1	1.268	7.181e-3	4.609e-3	2.767e-2
	2	1.902e-1	7.047e-2	8.675e-2	
3	1	1.259	8.002e-3	4.663e-3	2.617e-2
	2	2.091e-1	8.344e-2	1.021e-1	
4	1	1.259	8.002e-3	4.663e-3	2.617e-2
	2	2.091e-1	7.3324e-2	1.021e-1	
5	1	1.257	6.034e-4	0	4.754e-2
	2	1.592e-1	1.911e-2	0	

Table 2: Reference Material Properties for Benchmark Core

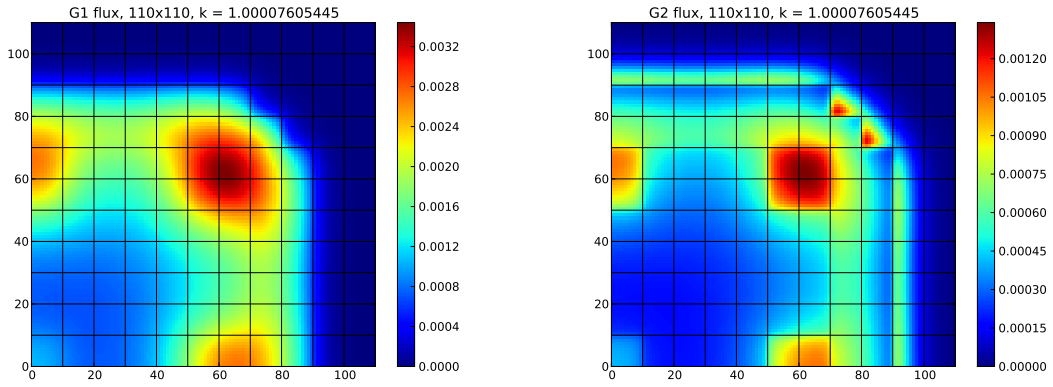

(a) ϕ, Group 1

(b) ϕ, Group 2

Figure 2: Reference Flux Profiles

3.5 Deterministic Solver

The criticality eigenvalue and quantity of interest $k(\phi)$ is converged on iteratively by

$$k^{n+1} = k^n \sum_{g=1}^{2} \frac{\iint\limits_{\Omega} \nu\Sigma_f^{(g)} \phi_g^{n+1}(\bar{x})\ d\bar{x}}{\iint\limits_{\Omega} \nu\Sigma_f^{(g)} \phi_g^{n}(\bar{x})\ d\bar{x}}. \tag{14}$$

until a convergence tolerance is achieved. We solve ϕ_1, ϕ_2, and k nonlinearly and simultaneously using a globally- and locally-conservative finite volume approximation in space. We solve implicitly with a Jacobian-Free Newton Krylov method, using a GMRES package from nonlinear solver package `trilinos` [2].

To verify the deterministic solver, we compare flux profiles and k to the original benchmark [4] as well as demonstrate the convergence of k with increasing mesh grid refinement. The deterministic solver is in agreement with the benchmark, and convergence for k and both group fluxes are demonstrated in Fig. 3. Both fluxes as well as the k-eigenvalue converge between first and second order. The finite volume method is second order, but the overall convergence order is reduced by first-order boundary condition treatments. In all cases, reducing the size of $h = \Delta x = \Delta y$ decreases the error in the solution. The reference solution is a level of refinement finer than the finest point shown. The flux error is calculated by considering the maximum error among several point-wise flux values, while k error is the global value for each refinement.

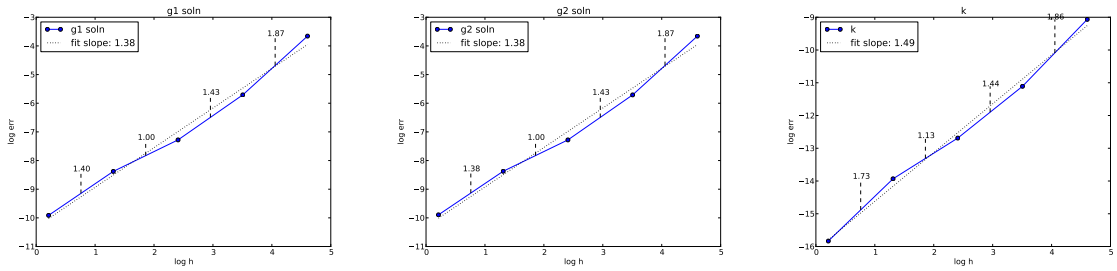

(a) ϕ, Group 1 (b) ϕ, Group 2 (c) k

Figure 3: Deterministic Solver Convergence

4 Uncertainty Quantification

Throughout the remainder of this document, we will represent the solution to the k-eigenvalue problem generically as $u(Y)$, where u corresponds to the value of k and Y is the vector of uncertain input parameters.

There are 33 total input parameters in Table 2 that can be treated as uncertain. For simplicity, any uncertainty introduced by these parameters is taken to be uniformly distributed within 10% of the reference value. We consider three cases for uncertainty quantification, distinguished chiefly by the number of input parameters with uncertainty (N): material 1 uncertainty, where all the material properties for material 1 are treated as uncertain (N=7); low-energy group uncertainty, where all material properties for group 2 are treated as uncertain (N=13); and full uncertainty, where all material properties are treated as uncertain (N=33).

The test for a method's effectiveness will be considering the level of error reached as a function of the number of calls to the deterministic solver required. While there is some difference in overhead cost between methods, this diminishes for sufficiently costly deterministic solutions.
In general, moments of the quantity of interest $u(Y)$ are obtained by

$$\mathbb{E}[u(Y)^r] = \int_\Gamma u(Y)^r P(Y) dY, \tag{15}$$

where r is the desired moment, $Y = [Y_1, Y_2, \ldots, Y_N]$ are the uncertain inputs, $P(Y)$ is the joint probability distribution of Y, and Γ is the uncertainty space spanned by Y.

4.1 Monte Carlo

By way of benchmark, we consider analog Monte Carlo (MC) as a benchmark uncertainty quantification technique. Analog Monte Carlo determines the moments of a function by randomly sampling from the uncertainty space repeatedly until an accurate idea of the result is obtained. Monte Carlo benefits from a guaranteed consistent rate of convergence; however, this convergence rate is quite low; it typically converges as 1 over the square root of the number of deterministic solves. MC approximates moments of $u(Y)$ as

$$\mathbb{E}[u(Y)^r] \approx \frac{1}{\eta} \sum_{m=1}^{\eta} u(Y^{(m)})^r, \tag{16}$$

where η is the total number of samples taken, m is the index of a sample, and $Y^{(m)}$ is a point randomly sampled from Γ.

4.2 Stochastic Collocation

In stochastic collocation, we approximate $u(Y)$ as the sum of u evaluated at η collocated points multiplied by multidimensional Lagrangian polynomials. We make use of the quadrature index k, not to be confused with the criticality factor $k(Y)$ (represented by $u(Y)$).

$$u(Y) \approx u_{h,\eta,\Lambda(L)}(Y) = \sum_{k=0}^{\eta} u(Y^{(k)}) \mathcal{L}_k(Y), \tag{17}$$

$$\mathcal{L}_k(Y) = \prod_{n=1}^{N} \mathcal{L}_{k_n}(Y_n), \tag{18}$$

$$\mathcal{L}_{k_n}(Y_n) = \prod_{j=1}^{i} \frac{Y_n - Y_n^{(i)}}{Y_n^{(k_n)} - Y_n^{(i)}}, \tag{19}$$

$$\mathbb{E}[u(Y)] \approx \mathbb{E}[u_h(Y)] = \sum_{k=1}^{\eta} w_k \; u_h\Big(Y^{(k)}\Big), \tag{20}$$

where $u_h(Y)$ is the spatially-discretized PDE solution, and $Y^{(k)} = [Y^{(k_1)}, \cdots, Y^{(k_N)}]$ are realizations of Y similar to Y_m in Monte Carlo but chosen at quadrature points $Y^{(k)}$ with corresponding weights w_k. For this study, uniformly-distributed uncertain parameters suggest Gauss-Legendre quadrature to obtain collocation points and weights. The necessary quadrature points are obtained based on polynomial expansion orders from an index set $\Lambda(L)$.

4.2.1 Index Set $\Lambda(L)$

The index set $\Lambda(L)$ provides the basis for most of the polynomial representation, including determining the quadrature set to evaluate the sum in Eq. 17. L is the polynomial degree of the stochastic collocation expansion. For example, for a single uncertain parameter ($N = 1$) and a fourth-order polynomial approximation ($L = 4$), Λ includes all polynomial orders from 0 to 4, ($\Lambda = [0, 1, 2, 3, 4]$). Each index point $p \in \Lambda$ corresponds to a polynomial expansion moment of order i.

In the multivariate case, there are several methods to determine what index set to use. In the most naive case, $\Lambda(L)$ is a tensor product of polynomial expansion orders,

$$\Lambda_{\mathrm{TP}}(L) = \Big\{\bar{p} = [p_1, ..., p_N] : \max_{1 \le n \le N} p_n \le L\Big\}, \quad |\Lambda_{\mathrm{TP}}(L)| = (L+1)^2. \tag{21}$$

For example, for $N = 2$ and $L = 4$, the index set $\Lambda_{\mathrm{TP}}(L)$ includes all combinations of the expansion orders $[0, 1, 2, 3, 4] \otimes [0, 1, 2, 3, 4]$ for a total of 25 polynomial expansion indices. The collection of expansion points in this example index set is shown in Fig. 4a.

Other index sets with less cardinality can be employed to reduce the number of collocation points. Two in particular are the "total degree" set (see Fig. 4b), which is ideal for quantities that are analytic in stochastic space,

$$\Lambda_{\mathrm{TD}}(L) = \Big\{\bar{p} = [p_1, ..., p_N] : \sum_{n=1}^{N} p_n \le L\Big\}, \quad |\Lambda_{\mathrm{TD}}(L)| = \binom{L+N}{N}, \tag{22}$$

and the "hyperbolic cross" index set (see Fig. 4c), for quantities that have limited smoothness in stochastic space,

$$\Lambda_{\mathrm{HC}}(L) = \left\{\bar{p} = [p_1, ..., p_N] : \prod_{n=1}^{N} p_n + 1 \leq L + 1\right\}, \quad |\Lambda_{\mathrm{HC}}(L)| \leq (L+1)(1+\log(L+1))^{N-1}. \quad (23)$$

Figure 4 shows each of these index sets for $N = 2, L = 4$. The savings of total degree and hyperbolic cross help fight the curse of dimensionality present in tensor product.

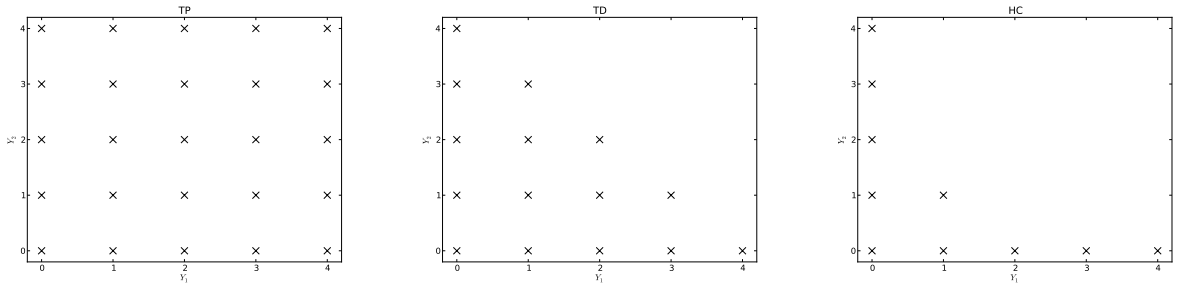

(a) Tensor Product (b) Total Degree (c) Hyperbolic Cross

Figure 4: Index Set Examples: $N = 2, L = 4$

4.2.2 Sparse Grid Quadrature

The collocation points used in the Lagrange polynomial expansion are obtained based on the index set chosen. To uniquely specify an isotropic Smolyak-like sparse grid, it is necessary to determine the number of uncertain variables N, the desired expansion order L, the index set $\Lambda(L)$, the quadrature rule $p(i)$, and the quadrature points-and-weights generating function for one-dimensional quadratures. This provides the isotropic sparse grid approximation

$$u(Y) \approx \mathcal{S}_{N,\Lambda(L)}[k](Y) = \sum_{\boldsymbol{i} \in \Lambda(L)} c(\boldsymbol{i}) \bigotimes_{n=1}^{N} \mathcal{U}_{n,p(i_n)}[u](Y), \quad (24)$$

$$c(\boldsymbol{i}) = \sum_{\substack{\boldsymbol{j} = \{0,1\}^N, \\ \boldsymbol{i}+\boldsymbol{j} \in \Lambda(L)}} (-1)^{|\boldsymbol{j}|_1}, \quad (25)$$

$$\bigotimes_{n=1}^{N} \mathcal{U}_{n,p(i_n)}[u](Y) \equiv \sum_{k_1=0}^{p(i_1)} \cdots \sum_{k_N=0}^{p(i_N)} u_h\left(Y^{(k_1)}, \cdots, Y^{(k_N)}\right) \prod_{n=1}^{N} \mathcal{L}_{k_n}(Y_n), \quad (26)$$

$$= \sum_{k}^{p(\vec{i})} u_h\left(Y^{(k)}\right) \mathcal{L}_k(Y), \quad (27)$$

where $p(i)$ is the "quadrature rule" used to obtain the number of quadrature points for a given expansion order. While this can be chosen arbitrarily, it is common to select $p(i) = i$ for Gauss quadrature and $p(i) = 2^i$ for Clenshaw-Curtis quadrature. The sparse grid quadrature is obtained through the tensor product of smaller quadratures, which has less cardinality than the full tensor quadrature. The savings in collocation points are demonstrated in Figure 5 for two identically

distributed uniform variables, each on [-1,1]. The reduction in collocation points grows with the number of input parameters N and the expansion order L. A visual example of sparse grids for two variables uniformly distributed between -1 and 1 using Gauss-Legendre quadrature is shown in Fig. 5.

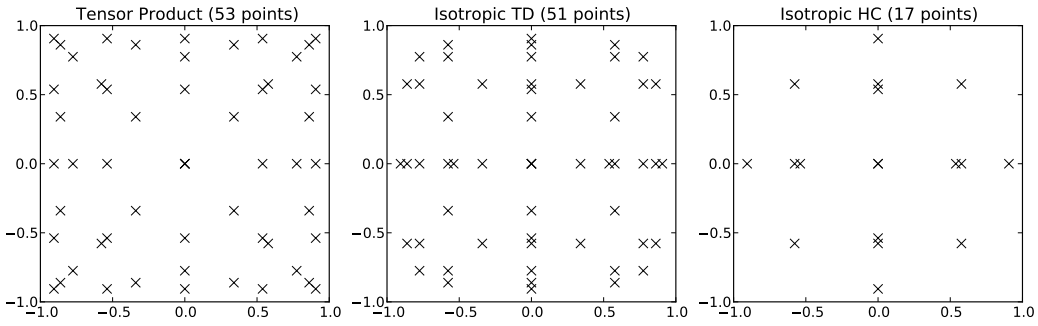

Figure 5: Sparse Grids, $N = 2, L = 4, p(i) = i$, Legendre points

For comparison, we show the number of index points for two input spaces of dimensionality N and several expansion levels L for all three index sets, as well as the number of collocation points for total degree and hyperbolic cross rules in Table 3. We note that accuracy cannot be directly drawn from polynomial expansions; for this problem the same number of collocation points results in a similar magnitude error in both total degree and hyperbolic cross. This implies, for this problem, that a much lower-order polynomial expansion constructed using the total degree rule is comparable in error to a larger-order polynomial expansion constructed using the hyperbolic cross rule.

N	L	TP	TD		HC	
		$\|\Lambda(L)\|$	$\|\Lambda(L)\|$	η	$\|\Lambda(L)\|$	η
3	4	125	35	165	16	31
	8	729	165	2,097	44	153
	16	4,913	969	41,857	113	513
5	2	293	21	61	11	11
	4	3,125	126	781	31	71
	8	59,049	1,287	28,553	111	481

Table 3: Index Set and Collocation Size Comparison

While the hyberbolic cross collocation points are significantly more sparse than the total degree collocation points, we note that the increased number of polynomial expansion moments in total degree make it much more accurate for the same total polynomial expansion level L. The results of this work demonstrate that for this problem, the same number of collocation points using either total degree or hyperbolic cross results in a similar magnitude of error.

4.3 Attenuation Problem Results

Figures 6 and 7 show the improvement of the various UQ methods discussed as a function of the number of deterministic solves required. Because each variable contributes identically, anisotropic methods did not show any improvement over collocation. Given the unlimited smoothness of the uncertainty space, we are not surprised to see the total degree sparse grid for stochastic collocation outperform both Monte Carlo and hyperbolic cross sparse grid.

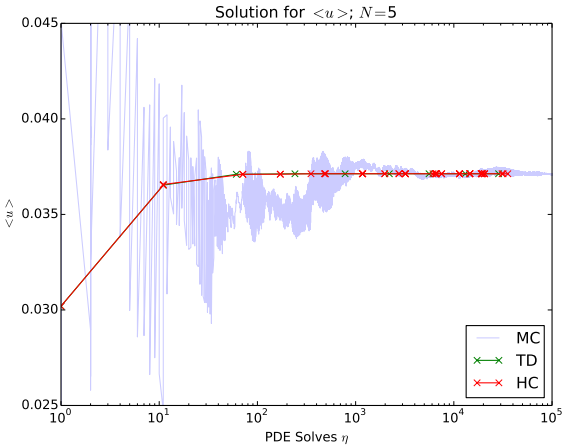

Figure 6: $< u >$ Values

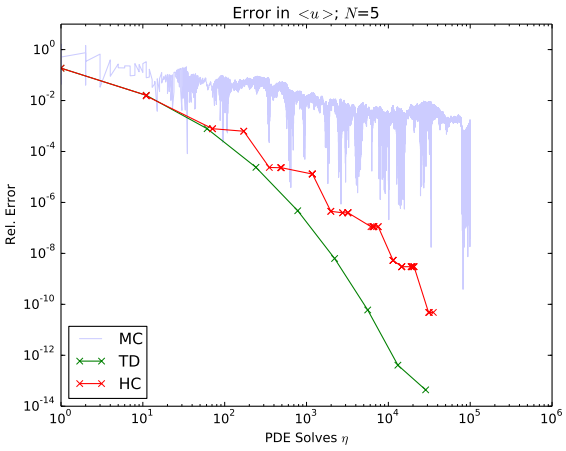

Figure 7: Error in $< u >$

4.4 Projectile Problem Results

Figures 8 and 9 show the improvement of the various UQ methods discussed as a function of the number of deterministic solves required. Because each variable contributes identically, anisotropic methods did not show any improvement over collocation. The uncertainty space for this problem is significantly less smooth than for the analytic attenuation problem, so we see hyperbolic cross converging more efficiently than total degree.

There are two particular points of interest in Figure 9. First, there is a vertical drop in error at $\eta = 11$ solves. For hyperbolic cross, it is not uncommon for a higher-order polynomial set to require the same number of computational solves as the polynomial order just smaller in order, and yet increase accuracy. This comes from spending less effort on resolving interactions between uncertainties and more effort on resolving contributions from single inputs. Second, there is oscillation in the error convergence below an error of about 10^{-5}. This is an artifact that arises from the deterministic solver. Because of the forward-Euler method of the solver, it converges only as well as the time step

selected. In this case, the relative error converged to in the deterministic solver time step was on the order of 10^{-5}, so the stochastic solver cannot converge the uncertain space any further, and any apparent convergence is incidental. Tightening the tolerance in the deterministic solver extends the convergence range of the stochastic solver.

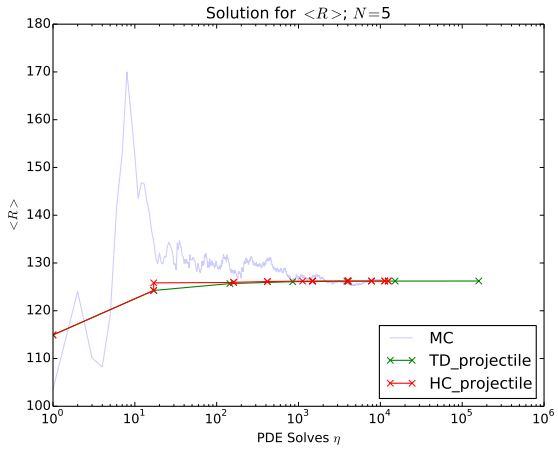

Figure 8: $< R >$ Values

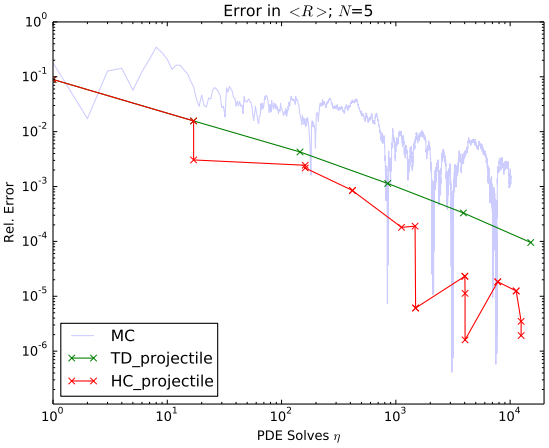

Figure 9: Error in $< R >$

4.5 Diffusion Solver Results

In order to compare magnitude of error, we use a "benchmark" solution generated with a high number of collocation points using isotropic sparse grid stochastic collocation as a reference solution. Monte Carlo and stochastic collocation solutions for varying numbers of PDE solves are computed, and relative error is plotted as a function of number of solves. The error is in the moments r of the quantity of interest $k(Y) = u(Y)$, and is given by

$$\epsilon_h^{(r)} = \frac{|\mathbb{E}[u^{(r)}] - \mathbb{E}[u_{\text{ref}}^{(r)}]|}{\mathbb{E}[u_{\text{ref}}^{(r)}]}, \tag{28}$$

$$\mathbb{E}[u^{(r)}] \approx \mathbb{E}[S_{N,\Lambda_{\mathrm{TD}}(L)}[u](Y)^{(r)}] = \sum_{k=1}^{\eta} w_k \; u^{(r)}\left(Y^{(k)}\right), \tag{29}$$

where the weights w_k and points $Y^{(k)}$ come from the multivariate quadrature used in stochastic collocation.

Figs. **??**-11 show the comparison of Monte Carlo convergence to stochastic collocation for $N = 1, 3, 5$ where N is the number of uncertain parameters. Both total degree (TD) and hyperbolic cross (HC) index sets have been included for $N > 1$ (they are indistinguishable for $N = 1$). Additionally, we include two low-anisotropy anisotropic grids.

Because of the regularity of $k(Y) = u(Y)$, the total degree index set is as cost effective as the hyperbolic cross index set. For a less regular stochastic solution, we expect hyperbolic cross would be more efficient. We also expect the convergence rate to diminish with increasing N, and that trend can be seen in the figures for the mean and variance of $k(Y)$. Both the magnitude of the error as well as the convergence rate of stochastic collocation outperforms Monte Carlo for any number of runs. In addition, heuristic selection of importance weighting improved the accuracy of sparse grid methods by approximately half an order of magnitude.

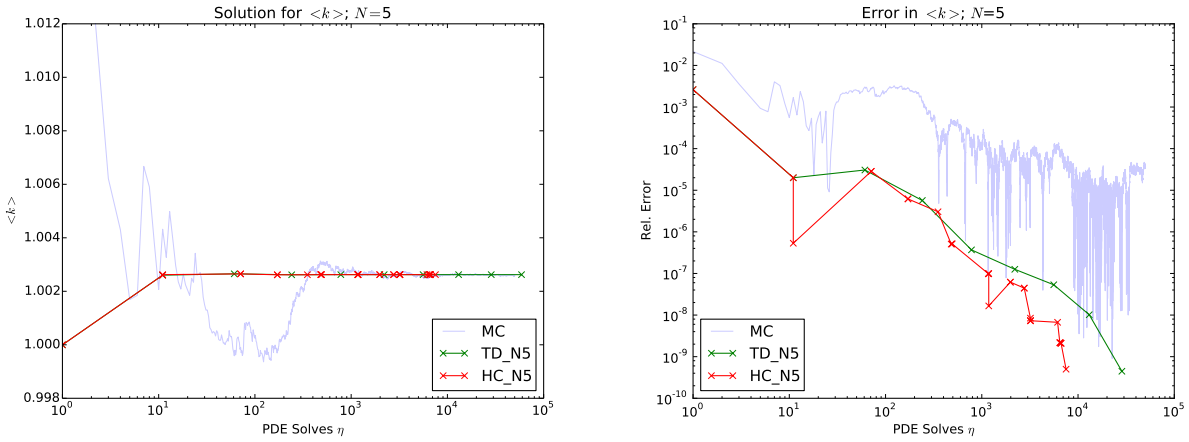

(a) Values (b) Errors

Figure 10: Diffusion, $N = 5$, Mean

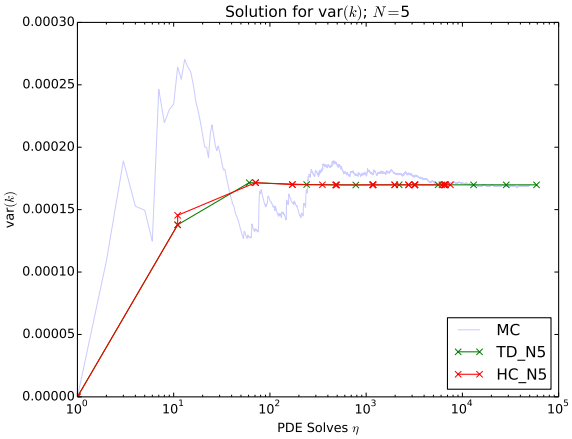

(a) Values

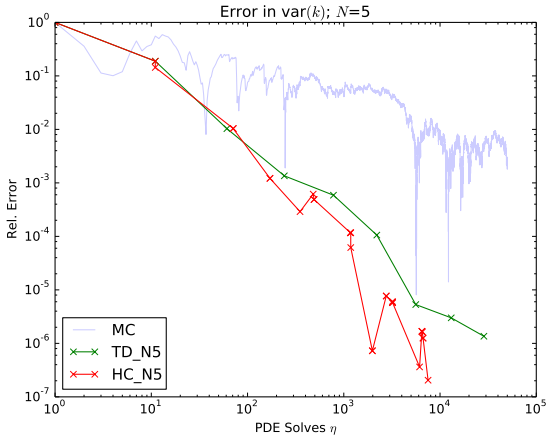

(b) Errors

Figure 11: Diffusion, $N = 5$, Variance

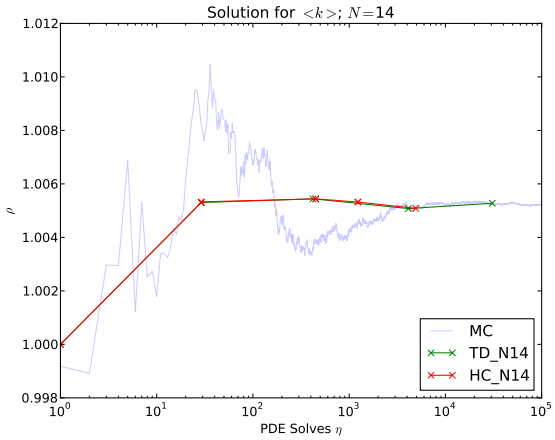

(a) Values

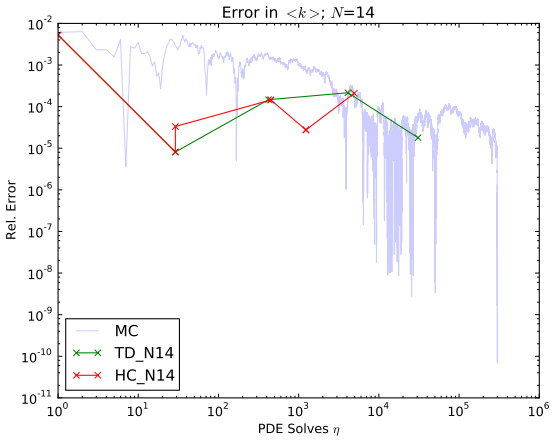

(b) Errors

Figure 12: Diffusion, $N = 14$, Mean

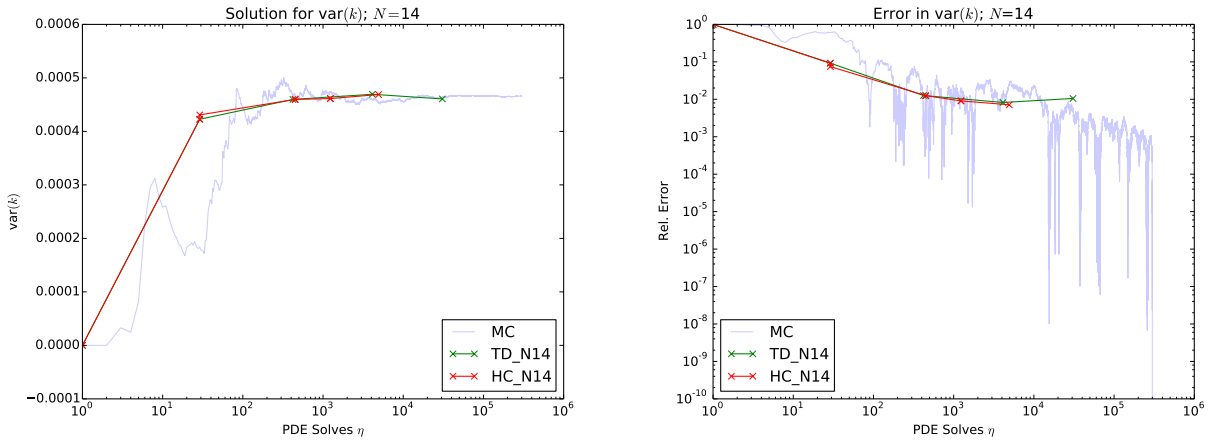

(a) Values (b) Errors

Figure 13: Diffusion, $N = 14$ Variance

5 Additional Improvements

Besides using sparse grid quadrature for stochastic collocation, there are a number of other approaches to stochastic collocation that can further reduce the sample space and improve convergence.

5.1 Anisotropic Sparse Grid

One disadvantage of sparse grids as defined above is that it treats all dimensions of uncertainty space equally. In many cases, however, the sensitivity of the stochastic solution to one dimension is less than another. For example, we heuristically expect the sensitivity of the k-eigenvalue to the reflecting material (material 5) diffusion coefficient to be much less than the sensitivity to the fission cross section in the main fissile material (material 1).

We can leverage the varying sensitivity by introducing importance parameters $\vec{\alpha} = [\alpha_1, \cdots, \alpha_N]$ that parametrize the sensitivity of the stochastic solution to each dimension. Using the one-norm

$$|\vec{\alpha}|_1 \equiv \frac{1}{N} \sum_{n=1}^{N} \alpha_n, \tag{30}$$

these weight parameters adjust the index set rules $\Lambda(L)$ for total degree and hyperbolic cross as

$$\tilde{\Lambda}_{\mathrm{TD}}(L) = \left\{ \bar{p} = [p_1, ..., p_N] : \sum_{n=1}^{N} \alpha_n p_n \leq |\vec{\alpha}|_1 L \right\}, \tag{31}$$

$$\tilde{\Lambda}_{\mathrm{HC}}(L) = \left\{ \bar{p} = [p_1, ..., p_N] : \prod_{n=1}^{N} (p_n + 1)^{\alpha_n} \leq (L+1)^{|\vec{\alpha}|_1} \right\}. \tag{32}$$

In this formulation, greater values of α_n result in less quadrature points for uncertain input Y_n. Smaller values of α_n are assigned to more sensitive dimensions to prioritize collocation points.

5.2 HDMR

Despite the gains in efficiency from using anisotropic sparse grids, stochastic collocation still suffers from the curse of dimensionality, becoming computationally unwieldy for more than a dozen uncertain inputs. We can further improve the efficiency of deterministic uncertainty quantification by making use of high-density model reduction (HDMR) techniques [5]. These methods have been applied recently to neutronics problems for significant gain in efficiency [3].

Cut-HDMR makes use of representative "slices" or cuts of the uncertainty space. This slice in uncertainty space makes use of "reference values" for each of the uncertain inputs, often the mean or most likely value for the parameter. We denote the reference value for input parameter Y_n as $Y_n^{(0)}$. Cut-HDMR uses reference values for the majority of inputs at a time and varies small numbers of parameters, then constructs the results as a linear sum of the contributions. It approximates a function as a sum of increasing interactions,

$$u(Y) = H[u](Y) = u_0 + \sum_{n_1=1}^{N} u_{n_1} + \sum_{n_1=1}^{N}\sum_{n_2=1}^{n_1} u_{n_1,n_2} + \sum_{n_1=1}^{N}\sum_{n_2=1}^{n_1}\sum_{n_3=1}^{n_2} u_{n_1,n_2,n_3} + ..., \tag{33}$$

$$u_0 = u(Y^{(0)}), \tag{34}$$

$$u_n \equiv u(Y_n) - u_0, \tag{35}$$

$$u_{i,j} \equiv u(Y_i, Y_j, \bar{Y}) - u_i - u_j - u_0, \tag{36}$$

and so on. Here N is the total number of uncertain inputs, and

$$u(Y_n) = u\big|_{Y_i = Y_i^{(0)}, i \neq n} \equiv u(Y_1^{(0)}, Y_2^{(0)}, \ldots, Y_n, \ldots, Y_N^{(0)}), \tag{37}$$

indicates holding any variables not explicitly listed at the reference value. For multiple listed uncertain inputs,

$$u(Y_m, Y_n) \equiv u(Y_1^{(0)}, Y_2^{(0)}, \ldots, Y_m, \ldots, Y_n, \ldots, Y_N^{(0)}), \tag{38}$$

This Cut-HDMR representation allows us to approximate by truncating at a particular interaction level H. For instance, an $H2$ approximation would only include the terms

$$u(Y) \approx H_2[u](Y) = u_0 + \sum_{i}^{N} u_i + \sum_{i}^{N}\sum_{j}^{i-1} u_{i,j}. \tag{39}$$

A variety of methods can be used to represent $u(Y)$. In our case, we make use of stochastic collocation on sparse grids, which is most efficient for a moderate number of uncertain inputs. For example,

$$u(Y) \approx H_2[u](Y) \approx S_0 + \sum_{i}^{N} S_i + \sum_{i}^{N}\sum_{j}^{i-1} S_{i,j}, \tag{40}$$

$$S_0 \equiv S[u](\bar{Y}), \tag{41}$$

$$S_i \equiv S[u](Y_i, \bar{Y}) - S_0, \tag{42}$$

$$S_{i,j} \equiv S[u](Y_i, Y_j, \bar{Y}) - S_i - S_j - S_0. \tag{43}$$

Moments r of this HDMR approximation can be obtained simply as - TODO is this true? -

$$\mathbb{E}[u(Y)^r] = \mathbb{E}[H[u](Y)^r] = u_0^r + \sum_{i}^{N} u_i^r + \sum_{i}^{N}\sum_{j}^{i} u_{i,j}^r + ... \tag{44}$$

5.2.1 Attenuation Problem Results

Figures 21a and 21b compare the convergence of the additional methods described here as a function of the number of deterministic solves required. Because each variable contributes identically, anisotropic methods did not show any improvement over collocation and are omitted for this problem. We note that, for five input parameters, it appears HDMR at best can tie the uncertainty convergence obtained by full collocation. This is sensible, as using sparse grid quadrature already removes most of the higher-order interactions between variables from consideration. We expect that as the number of input parameters increases, the benefit of HDMR will as well.

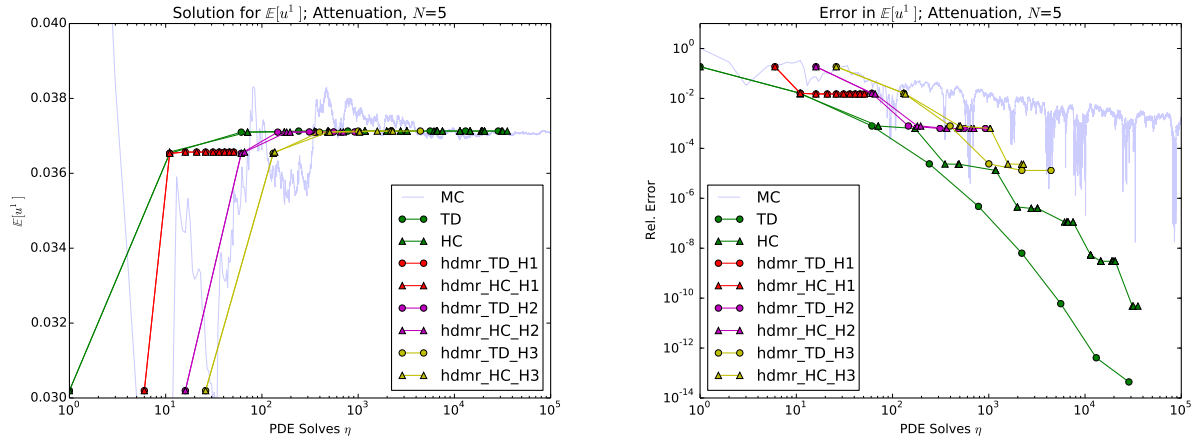

(a) $< u >$ Values (b) Error in $< u >$

Figure 14: Attenuation UQ Results, Mean

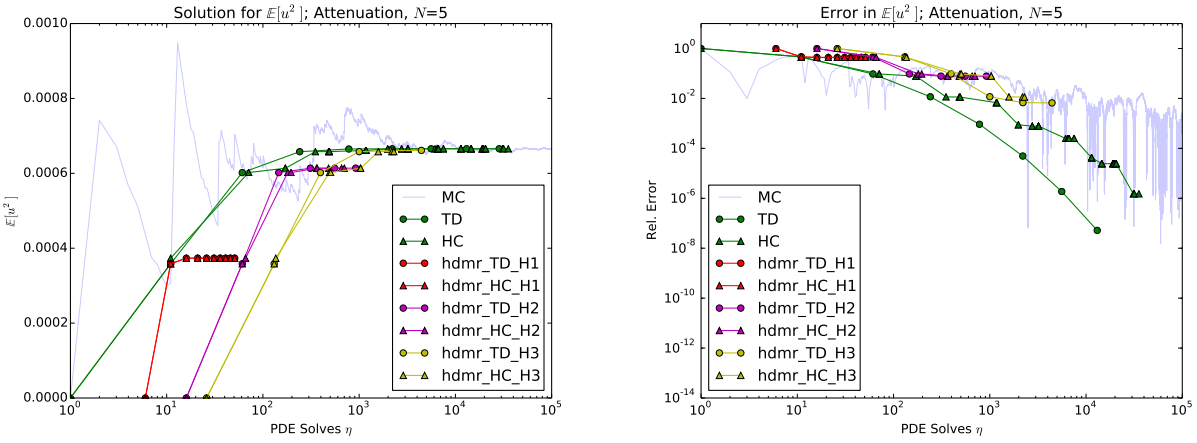

(a) $< u >$ Values (b) Error in $< u >$

Figure 15: Attenuation UQ Results, Variance

5.2.2 Projectile Problem Results

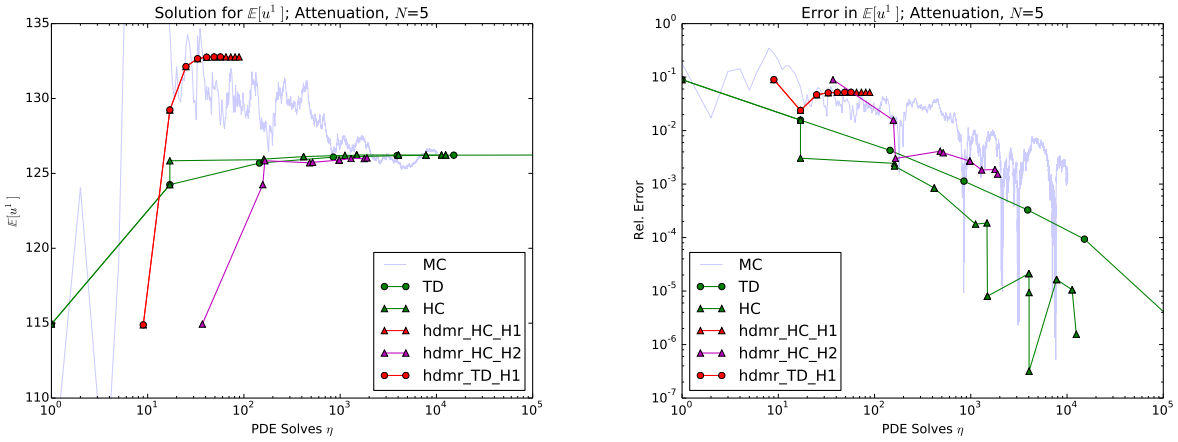

(a) $< u >$ Values (b) Error in $< u >$

Figure 16: Projectile UQ Results, Mean

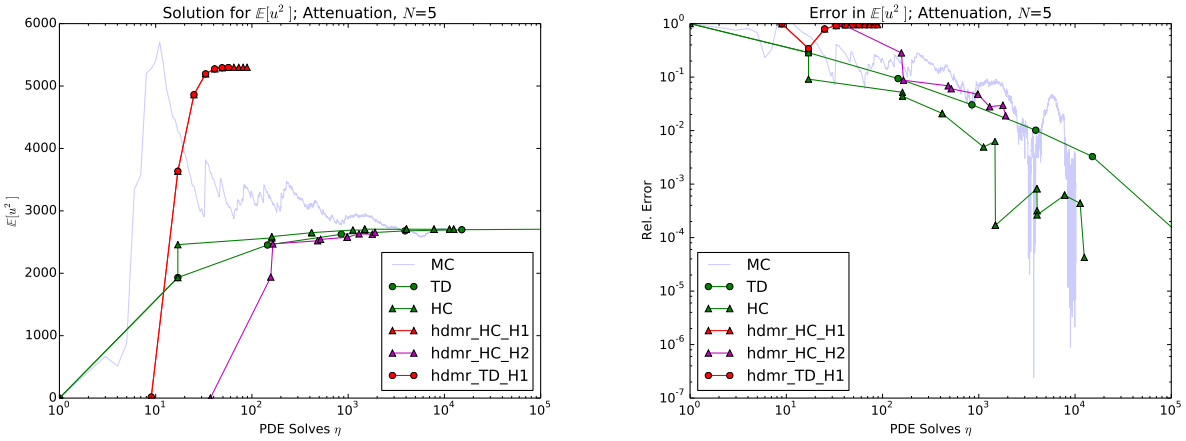

(a) $< u >$ Values (b) Error in $< u >$

Figure 17: Projectile UQ Results, Variance

5.2.3 Diffusion Problem Results

5.3 Anisotropic Sparse Grid

One disadvantage of sparse grids as defined above is that it treats all dimensions of uncertainty space equally. In many cases, however, the sensitivity of the stochastic solution to one dimension is less than another. For example, we heuristically expect the sensitivity of the k-eigenvalue to the reflecting material (material 5) diffusion coefficient to be much less than the sensitivity to the fission cross section in the main fissile material (material 1).

We can leverage the varying sensitivity by introducing importance parameters $\vec{\alpha} = [\alpha_1, \cdots, \alpha_N]$ that

parametrize the sensitivity of the stochastic solution to each dimension. Using the one-norm

$$|\vec{\alpha}|_1 \equiv \frac{1}{N}\sum_{n=1}^{N}\alpha_n, \tag{45}$$

these weight parameters adjust the index set rules $\Lambda(L)$ for total degree and hyperbolic cross as

$$\tilde{\Lambda}_{\mathrm{TD}}(L) = \left\{\bar{p} = [p_1, ..., p_N] : \sum_{n=1}^{N}\alpha_n p_n \leq |\vec{\alpha}|_1 L\right\}, \tag{46}$$

$$\tilde{\Lambda}_{\mathrm{HC}}(L) = \left\{\bar{p} = [p_1, ..., p_N] : \prod_{n=1}^{N}(p_n+1)^{\alpha_n} \leq (L+1)^{|\vec{\alpha}|_1}\right\}. \tag{47}$$

In this formulation, greater values of α_n result in less quadrature points for uncertain input Y_n. Smaller values of α_n are assigned to more sensitive dimensions to prioritize collocation points.
One method to quantify the sensitivity of the quantity of interest to changes in each input parameter is by using an ANOVA-like approach with a well-converged HDMR calculation. We derive an importance factor based on the contribution of each single variable to the overall second moment.

$$\mathbb{E}[u(Y)^2] \approx \mathbb{E}[H_3[u](Y)^2] = u_0^2 + \sum_{n_1=1}^{N} u_{n_1}^2 + \sum_{n_1=1}^{N}\sum_{n_2=1}^{n_1} u_{n_1,n_2}^2 + \sum_{n_1=1}^{N}\sum_{n_2=1}^{n_1}\sum_{n_3=1}^{n_2} u_{n_1,n_2,n_3}^2, \tag{48}$$

$$\alpha_n = \mathrm{ceil}\left[-\log\left(\frac{u_n^2}{\mathbb{E}[H[u](Y)^2]}\right)\right]. \tag{49}$$

While not the only method for calculating weight factors, this formulation ensures positive integers with a minimum of 1 for each weight factor.

We omit results for the attenuation case, as each variable contributes identically and no anisotropy performs better than isotropic sparse grid for this case.

5.3.1 Projectile Problem

Table 4 shows values found using an order $H_1[u](Y)$ approximation for the projectile problem. The drag coefficient C is clearly the input with the most impact, while the gravitational acceleration constant g has the least effect. We note that these sensitivities are based on the uncertain ranges given above; changing the uncertainty ranges or distribution could impact the weighting factors α. As shown in Figures 18 and 19, employing a variance-based anisotropic sparse grid collocation shows orders of magnitude improvement in convergence and overall error when compared to isotropic sparse grid collocation.

Y_n	Y_n^2	$\frac{Y_n^2}{H_1^2[u](Y)}$	α_n
m	2.57E4	6.2E-5	5
r	2.61E4	6.3E-5	5
C	9.45E7	2.3E-1	1
ρ	1.52E3	3.6E-6	6
v	4.18E1	1.0E-7	7
θ	1.93E7	4.6E-2	2
g	2.77E-3	6.6E-12	12
y_i	1.56E4	5.7E-5	5

Table 4: Anisotropies for Projectile Problem

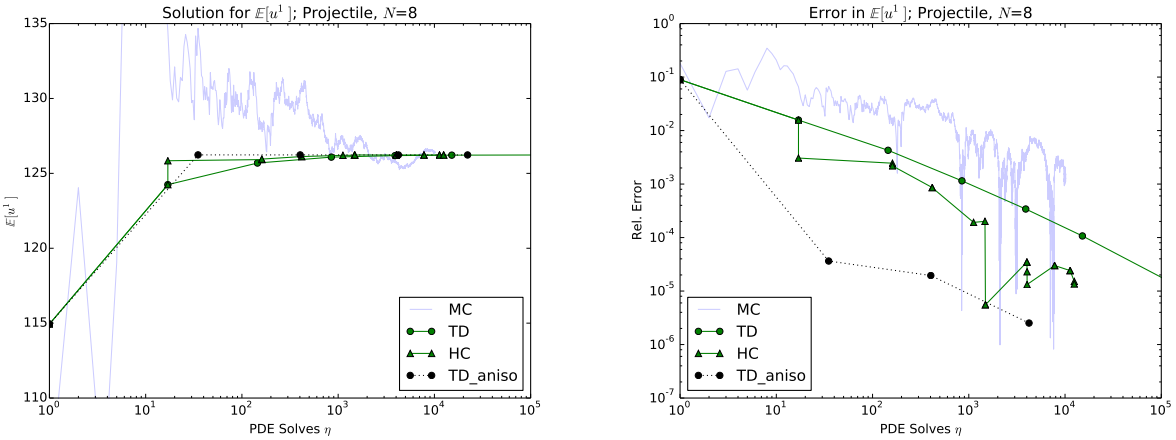

(a) Values (b) Error

Figure 18: Projectile UQ Results, Mean

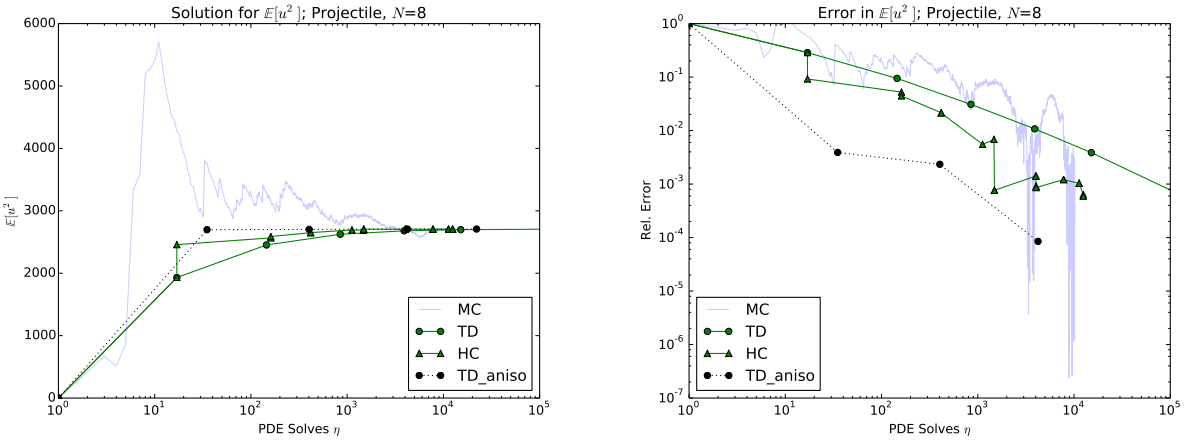

(a) Values (b) Error

Figure 19: Projectile UQ Results, Variance

5.3.2 Diffusion Problem, $N = 5$

Table **??** shows values found using an $H_1[u](Y)$ approximation for the projectile problem. As expected, the capture and fission cross sections in the most prevalent materials have the greatest effect on the k-eigenvalue.
As shown in Figures **??** and **??**, employing a variance-based anisotropic sparse grid collocation shows some improvement over an isotropic sparse grid.
TODO FIX THIS

Y_n	Y_n^2	$\frac{Y_n^2}{H_1^2[u](Y)}$	α_n
$D_2^{(1)}$	1.75E-13	1.8E-13	13
$\Sigma_{c,2}^{(1)}$	9.86E-6	9.9E-6	6
$\Sigma_{f,2}^{(1)}$	4.80E-6	4.8E-6	6
$D_2^{(4)}$	2.12E-14	2.1E-14	14
$\Sigma_{c,2}^{(4)}$	2.05E-9	2.1E-9	9
$\Sigma_{f,2}^{(4)}$	4.59E-10	4.6E-10	10
$D_2^{(5)}$	6.18E-13	6.2E-13	13

Table 5: Anisotropies for Projectile Problem

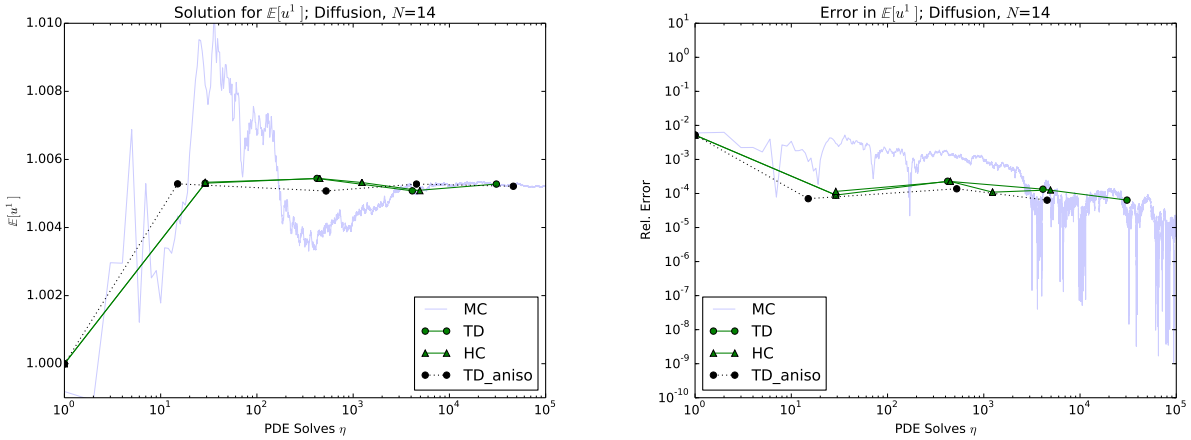

(a) Values

(b) Error

Figure 20: Diffusion ($N = 14$ UQ Results, Mean

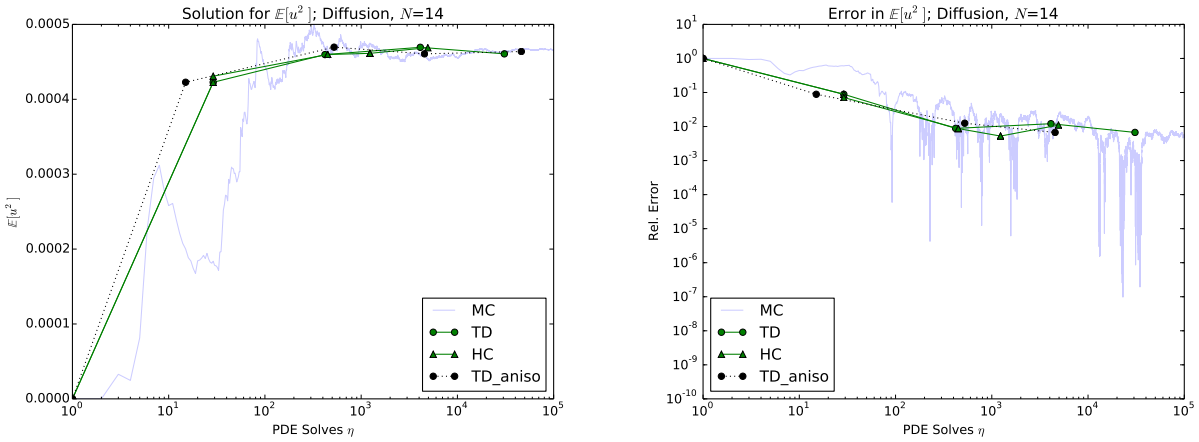

(a) Values

(b) Error

Figure 21: Projectile UQ Results, Variance

5.3.3 Diffusion Problem, $N = 14$

Table 5 shows values found using an $H_1[u](Y)$ approximation for the projectile problem. As expected, the capture and fission cross sections in the most prevalent materials have the greatest effect on the k-eigenvalue.

As shown in Figures 20 and 21, employing a variance-based anisotropic sparse grid collocation shows some improvement over an isotropic sparse grid.

Y_n	Y_n^2	$\frac{Y_n^2}{H_1^2[u](Y)}$	α_n
$D_2^{(1)}$	1.75E-13	1.8E-13	13
$\Sigma_{c,2}^{(1)}$	9.86E-6	9.9E-6	6
$\Sigma_{f,2}^{(1)}$	4.80E-6	4.8E-6	6
$D_2^{(2)}$	1.76E-13	1.8E-13	13
$\Sigma_{c,2}^{(2)}$	1.44E-6	1.4E-6	6
$\Sigma_{f,2}^{(2)}$	2.67E-7	2.7E-7	7
$D_2^{(3)}$	2.78E-14	2.8E-14	14
$\Sigma_{c,2}^{(3)}$	6.24E-6	6.2E-6	6
$\Sigma_{f,2}^{(3)}$	2.20E-6	2.2E-6	6
$D_2^{(4)}$	2.12E-14	2.1E-14	14
$\Sigma_{c,2}^{(4)}$	2.05E-9	2.1E-9	9
$\Sigma_{f,2}^{(4)}$	4.59E-10	4.6E-10	10
$D_2^{(5)}$	6.18E-13	6.2E-13	13
$\Sigma_{c,2}^{(5)}$	3.24E-10	3.2E-10	10

Table 6: Anisotropies for Projectile Problem

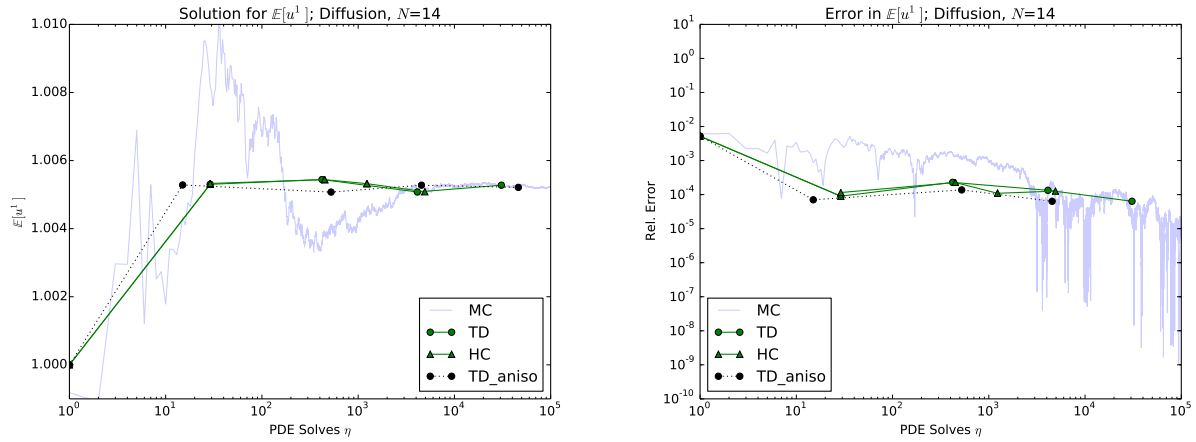

(a) Values (b) Error

Figure 22: Diffusion ($N = 14$ UQ Results, Mean

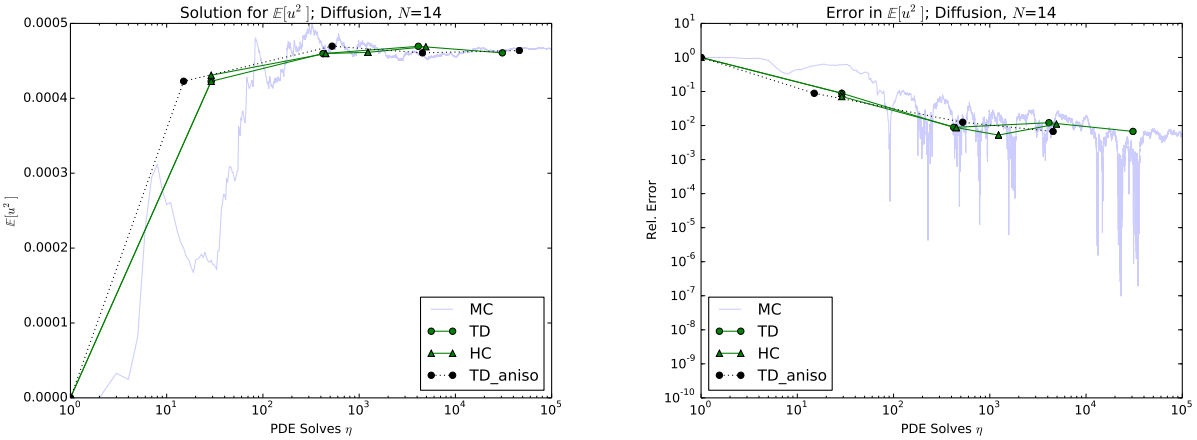

(a) Values (b) Error

Figure 23: Projectile UQ Results, Variance

6 Conclusion

TODO
Ongoing:

- Adaptive Anisotropic Sparse Grid
- Adaptive HDMR

7 Acknowledgments

This research was supported by research grants from Idaho National Laboratory.

References

[1] Ivo Babuska, Fabio Nobile, and Raul Tempone. A Stochastic Collocation Method for Elliptic Partial Differential Equations with Random Input Data. *SIAM Journal on Numerical Analysis*, 45, 2007.

[2] Michael Heroux et. al. An Overview of Trilinos. Technical Report SAND2003-2927, Sandia National Laboratories, 2003.

[3] Zhengzheng Hu, Ralph C. Smith, Jeffrey Willert, and C. T. Kelley. High Dimensional Model Representations for the Neutron Transport Equation. *NS&E*, 177, 2014.

[4] Argonne National Laboratory. Argonne code center: Benchmark problem book. *ANL-7416 M&C Division of ANS*, 1968.

[5] G. Li, C. Rosenthal, and H. Rabitz. High Dimensional Model Representations. *J. Phys. Chem. A*, 105, 2001.

[6] Nobile, Tempone, and Webster. A Sparse Grid Stochastic Collocation Method for Partial Differential Equations with Random Input Data. *SIAM Journal on Numerical Analysis*, 46, 2008.